

A method for minimizing the magnetic cross-talk in twin-aperture $\cos\theta$ superconducting dipoles

Alessandro Maria Ricci^{1,2,*} and Pasquale Fabbriatore^{2,†}

¹*Dipartimento di Fisica, Università di Genova, via Dodecaneso 33, I-16146 Genova, Italy*

²*INFN sezione di Genova, via Dodecaneso 33, I-16146 Genova, Italy*

(Dated: Wednesday 16th October, 2019, 00:50)

We present an analytic method to minimize the magnetic cross-talk in twin-aperture $\cos\theta$ dipoles. In the single-aperture $\cos\theta$ layout, the coil design can be performed with an analytic approach, based on a sector coil approximation. This method allows a fast evaluation of the field harmonics and an almost exhaustive scan on the positions and dimensions of the sectors, for coil layouts made of a different number of sectors. This increases the probabilities to find the coil shape which best fits the specifications. In a twin-aperture arrangement, the magnetic cross-talk can be not negligible and, to the aim of an analytic minimization of the unwanted multipoles, an extension of the single-aperture sector model is required. This is the case of the recombination dipole D2 for the High Luminosity LHC and of the 16-T bending dipole for the Future Circular Collider (FCC). This analytical method has been used to find alternative coil designs for both dipoles.

Keywords: Superconducting accelerator magnets, sector coils, cross-talk, field harmonics, High Luminosity Large Hadron Collider (HL-LHC), Future Circular Collider (FCC).

I. INTRODUCTION

The superconducting dipoles, bending the particle beams in the high energy accelerators, must provide a high-homogeneous magnetic field. The general rule is that any higher order multipole must be lower than 10^{-4} of the central field. Moreover, it is necessary to take into account many constraints on the coil shape (minimum bending radius, maximum magnet dimensions, inter-layer spacers, etc.), the costs, the operating margins, the effects of the persistent currents and the magnetic components, introducing difficulties in the design.

The colliders built so far (Tevatron, HERA, RHIC and LHC) used NbTi $\cos\theta$ dipole magnets. In this layout, the coil shape is an annulus and the conductors are piled up in blocks, separated by spacers and carrying the same constant current density [1–3]. This practical arrangement aims to approximate an ideal annulus, crossed by a current density proportional to the cosine of the azimuth ($\cos\theta$ annulus). This configuration is the most efficient in the use of superconducting material. However, different coil designs ($\cos\theta$ [4], common-coil [5], block-coil [6, 7] and canted- $\cos\theta$ [8]) were tested in Nb₃Sn to overcome manufacturing challenges and manage the stress. A summary for Nb₃Sn superconducting dipoles can be found in Ref. [9].

In the colliders two particle beams are counter-rotating and require two separate channels with opposite magnetic fields. Tevatron, HERA and RHIC have two separate storage rings and the superconducting magnets are designed with the beam pipe surrounded by the coil inside the iron yoke (single-aperture layout). The available

space in the LHC tunnel does not allow two separate storage rings. Thus, the main dipoles (MB), the main quadrupoles (MQ) and some magnets for the corrections, the insertion regions and the interaction regions are designed with the two beam pipes surrounded by the coils inside a common iron yoke [3, 10] (twin-aperture layout). In this configuration, each coil can generate unwanted multipoles in the other aperture (cross-talk). This problem is particularly important for a special class of dipoles involved in proximity of the collider Interaction Regions (IR), the recombination dipoles D2 [3, 10]. These special magnets are used for recombining the beams before the collision in the Interaction Point (IP). In order to achieve this, the magnetic field must have the same polarity in both apertures. In the LHC dipole D2, the 2.77-T magnetic field at the 188-mm inter-beam distance is high enough for generating a non-negligible cross-talk, but low enough for allowing the iron yoke to magnetically decouple the coils. However, this solution is no more viable in the new dipole D2 for the High Luminosity upgrade of LHC (HL-LHC) [11–14], because the higher magnetic field (4.5 T) saturates the iron yoke, resulting in a dramatic increase of the unwanted multipoles. Therefore, the iron yoke between the coils has been removed and the field quality is tuned by an asymmetric coil winding.

Recently, the Future Circular Collider Study (FCC) published the Conceptual Design Report (CDR) [15–18], which describes the feasibility of high-performance colliders, housed in a new 100-km tunnel in the area of Geneva. The hadron collider (FCC-hh) would achieve a 100-TeV collision energy and its Nb₃Sn bending dipoles would generate a 16-T magnetic field. Alternatively, the 16-T magnets could be used for a High Energy upgrade of the Large Hadron Collider (HE-LHC), which would increase the collision energy from 14 TeV to 27 TeV. The EuroCirCol Collaboration studied different designs [19–32] for the 16-T superconducting dipoles and chose as

* alessandro.ricci@ge.infn.it,
alessandromaria.ricci@edu.unige.it

† pasquale.fabbriatore@ge.infn.it

baseline the $\cos\theta$ layout [21, 32], whose coil cross-section is left-right asymmetric, because in the cold mass size constraint the elevate magnetic field leads to a strong cross-talk, which can be controlled only by an asymmetric coil winding.

In this paper we present an analytic method, which minimizes the magnetic cross-talk by finding the asymmetric coil cross-sections. The first step in the coil design is to find the block arrangements, which generate a high-homogeneous magnetic field given the bending radius, the cable width, the layer number and the inter-beam distance. These configurations cannot be derived explicitly and many numerical algorithms exist to find the optimal cross-sections [3]. Owing to the complicated magnet geometry (coils made of blocks, blocks made of cables and cables made of strands), they are time-consuming and, to be really effective, they have to operate on configurations which are not too far from a local optimum. Therefore, analytical models approximating the blocks as annular sectors (sector coil models) [1, 2, 33, 34] can be used to carry out an initial scan on a very large number of possible configurations [34–36]. This makes easier to find the cross-section which best suits the specifications. We extended the current sector model to analytically describe the contribution to the harmonic components, which one coil exerts on the other aperture. We used this extended sector model to find the asymmetric coil configurations, which minimize the cross-talk in the new dipole D2 of HL-LHC and in the 16-T bending dipole of FCC. In a computational time of few minutes for D2 and of few tens of minutes for the FCC dipole, this method allowed to find alternative magnetic designs, which have an excellent field quality. These results show that this method can be used as a complementary tool at the early stage of the coil design of a twin-aperture dipole, which presents a non-negligible cross-talk.

In Section II we review the current sector model, in Section III we explain the extended sector model and the resolving procedure, finally in Section IV we show the results.

II. THE CURRENT SECTOR MODEL

In the complex formalism, Biot and Savart's law set that a current line I in the position $z_0 \equiv x_0 + iy_0$ generates a magnetic field $B(z) \equiv B_y(z) + iB_x(z)$ in the position $z \equiv x + iy$ according to the formula

$$B(z) = \frac{\mu_0 I}{2\pi(z - z_0)}. \quad (1)$$

Knowing that for $|z| < 1$

$$\frac{1}{1 - z} = 1 + z + z^2 + z^3 + \dots = \sum_{n=1}^{\infty} z^{n-1}, \quad (2)$$

we can develop the multipolar expansion of the magnetic field for $|z| < |z_0|$, as

$$\begin{aligned} B(z) &= \frac{\mu_0 I}{2\pi(z - z_0)} = -\frac{\mu_0 I}{2\pi z_0} \frac{1}{1 - z/z_0} \\ &= -\frac{\mu_0 I}{2\pi z_0} \sum_{n=1}^{\infty} \left(\frac{z}{z_0}\right)^{n-1} \\ &= -\frac{\mu_0 I}{2\pi z_0} \sum_{n=1}^{\infty} \left(\frac{R_{ref}}{z_0}\right)^{n-1} \left(\frac{z}{R_{ref}}\right)^{n-1}, \end{aligned} \quad (3)$$

where R_{ref} is a reference radius usually chosen as $2/3$ of the aperture radius. We can re-write the multipolar expansion in the European notation as

$$B(x, y) = B_y + iB_x = \sum_{n=1}^{\infty} (B_n + iA_n) \left(\frac{x + iy}{R_{ref}}\right)^{n-1}, \quad (4)$$

where

$$\begin{aligned} B_n + iA_n &= -\frac{\mu_0 I}{2\pi z_0} \left(\frac{R_{ref}}{z_0}\right)^{n-1} \\ &= -\frac{\mu_0 I}{2\pi R_{ref}} \left(\frac{R_{ref}}{z_0}\right)^n. \end{aligned} \quad (5)$$

The coefficients A_n and B_n have the dimensions of the magnetic field (T) and they are called skew and normal cylindrical harmonics respectively. In the European definition (4), each component of order n represents the $2n$ -pole component. The cylindrical harmonics of a dipole can be dimensionless and normalized to units as $b_n = 10^4 B_n / B_1$ and $a_n = 10^4 A_n / B_1$, where B_1 is the dipole component generated from a current line, which follows from Eq. (5)

$$B_1 = -\frac{\mu_0 I}{2\pi} Re \left(\frac{1}{z_0}\right) = -\frac{\mu_0 I}{2\pi} \frac{x_0}{x_0^2 + y_0^2}. \quad (6)$$

Thus Eq. (4) becomes

$$B_y + iB_x = 10^{-4} B_1 \sum_{n=1}^{\infty} (b_n + ia_n) \left(\frac{x + iy}{R_{ref}}\right)^{n-1}, \quad (7)$$

where a_n and b_n are called normalized skew and normal cylindrical harmonics respectively.

Now let us consider the quadruplet of current lines (I, ρ, θ) , $(-I, \rho, \pi - \theta)$, $(-I, \rho, \pi + \theta)$, $(I, \rho, -\theta)$ shown in Fig. 1. The magnetic field generated by this quadruplet is the sum of the contributions of each current line and, within the circle of center O and radius ρ , it can be calculated by Eq. (4), where

$$\begin{aligned} B_n + iA_n &= -\frac{\mu_0 I}{2\pi R_{ref}} \left(\frac{R_{ref}}{\rho}\right)^n \\ &\times \left(e^{-in\theta} - e^{-in(\pi-\theta)} - e^{-in(\pi+\theta)} + e^{in\theta}\right). \end{aligned} \quad (8)$$

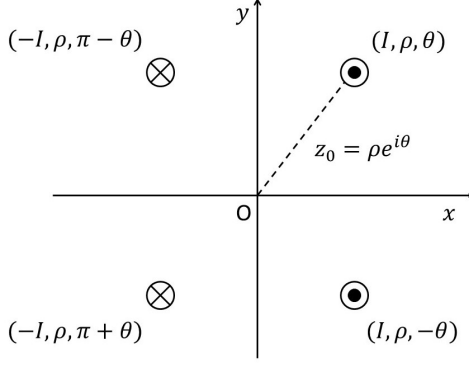


Figure 1. Quadruplet of current lines with an even symmetry about the x -axis and an odd symmetry about the y -axis.

Knowing that

$$\begin{aligned} e^{-in\theta} - e^{-in(\pi-\theta)} - e^{-in(\pi+\theta)} + e^{in\theta} \\ = 2[1 - (-1)^n] \cos n\theta, \end{aligned} \quad (9)$$

which is only non-zero when n is odd, the complex magnetic field can be written for $|z| < \rho$ with the only non-zero coefficients

$$B_n = \frac{2\mu_0 I}{\pi R_{ref}} \left(\frac{R_{ref}}{\rho} \right)^n \cos n\theta \quad n \text{ odd}, \quad (10)$$

which are called allowed cylindrical harmonics of this current distribution. The even symmetry about the x -axis deletes the skew harmonics and the odd symmetry about the y -axis drops the even normal harmonics.

Let us consider a dipole, whose quarter coil layout is a sector of width w and bending radius R , spanning the angle from 0 to ϕ . The layout is symmetric both about the x -axis and about the y -axis. A uniform current density J flows in the right half coil and $-J$ in the left (see Fig. 2). The allowed harmonics can be obtained by integrating the current in Eq. (10) over the sector:

$$B_n = \frac{2\mu_0 J R_{ref}^{n-1}}{\pi n (n-2)} \left(\frac{1}{(R+w)^{n-2}} - \frac{1}{R^{n-2}} \right) \sin n\phi. \quad (11)$$

Solving Eq. (11) we can find the angles that set to zero the first allowed harmonics B_3 and the ones that cancel the second allowed harmonics B_5 . Because the angles are different, we cannot have $B_3 = B_5 = 0$ with a single sector. If we consider a coil composed by two sectors $[0, \phi_1]$ and $[\phi_2, \phi_3]$, with a wedge between ϕ_1 and ϕ_2 , we can set $B_3 = B_5 = B_7 = 0$ by numerically solving the equation system

$$\sin 7\phi_3 - \sin 7\phi_2 + \sin 7\phi_1 = 0, \quad (12)$$

$$\sin 5\phi_3 - \sin 5\phi_2 + \sin 5\phi_1 = 0, \quad (13)$$

$$\sin 3\phi_3 - \sin 3\phi_2 + \sin 3\phi_1 = 0. \quad (14)$$

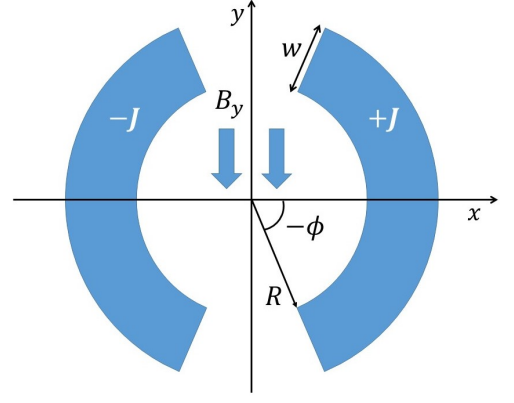


Figure 2. Sector coil layout for a dipole of inner radius R and coil width w , spanning the angle from 0 to ϕ . The layout is symmetric both about the x -axis and about the y -axis. In the right half coil a uniform current density J flows and in the left $-J$. The magnetic field for $r < R$ has the component B_y only.

At an early stage of the design process, we can use the sector coils to search the minimum number, the positions and the dimensions of the sector blocks, which meet the field quality requirements. This analytical model allows a very fast scan on a very large number of possible configurations.

III. THE EXTENDED SECTOR MODEL

The twin-aperture layout introduces a complicating factor, i.e. the contribution to the harmonic components which one coil exerts on the other aperture. This cross-talk can bring to non-zero normal coefficients also for even orders. To control the even normal harmonics we must break the symmetry of the current lines about the y -axis. Therefore, we consider a quadruplet of current lines, which is symmetric only about the x -axis (see Fig. 3). The normal multipoles can be written as

$$\begin{aligned} B_n = & -\frac{\mu_0 I}{\pi R_{ref}} \left(\frac{R_{ref}}{\rho} \right)^n \cos n\theta_1 \\ & - \frac{\mu_0 (-I)}{2\pi R_{ref}} \left(\frac{R_{ref}}{\rho} \right)^n \cos n(\pi - \theta_2) \\ & - \frac{\mu_0 (-I)}{2\pi R_{ref}} \left(\frac{R_{ref}}{\rho} \right)^n \cos n(\pi + \theta_2). \end{aligned} \quad (15)$$

Knowing that

$$\begin{aligned} \cos n(\pi - \theta_2) &= (-1)^n \cos n\theta_2, \\ \cos n(\pi + \theta_2) &= (-1)^n \cos n\theta_2, \end{aligned} \quad (16)$$

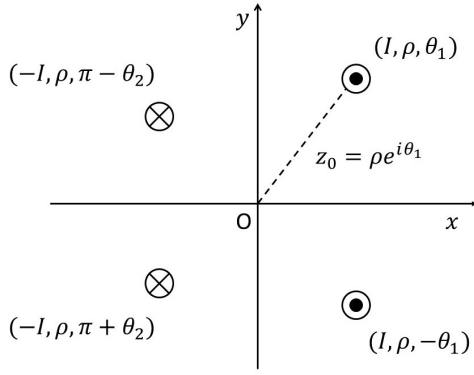


Figure 3. Asymmetric quadruplet of current lines about the y -axis and with an even symmetry about the x -axis.

Eq. (15) becomes

$$B_n = -\frac{\mu_0 I}{\pi R_{ref}} \left(\frac{R_{ref}}{\rho} \right)^n \times [\cos n\theta_1 - (-1)^n \cos n\theta_2]. \quad (17)$$

Integrating the current for passing to an asymmetric sector coil about the y -axis, we obtain

$$B_n = -\frac{\mu_0 J R_{ref}^{n-1}}{\pi} \int_R^{R+w} \frac{1}{\rho^{n-1}} d\rho \times \left(\int_\phi^{\phi'} \cos n\theta_1 d\theta_1 - (-1)^n \int_\psi^{\psi'} \cos n\theta_2 d\theta_2 \right), \quad (18)$$

where ϕ and ϕ' are the starting and final angles respectively for the right sector and ψ and ψ' are the starting and final angles respectively for the left sector. We get for $n \neq 2$

$$B_n = \frac{\mu_0 J R_{ref}^{n-1}}{\pi n (n-2)} \left(\frac{1}{(R+w)^{n-2}} - \frac{1}{R^{n-2}} \right) \times \left[\sin n\phi' - \sin n\phi - (-1)^n (\sin n\psi' - \sin n\psi) \right], \quad (19)$$

and for $n = 2$

$$B_2 = \frac{\mu_0 J R_{ref}}{2\pi} \ln \frac{R}{R+w} \times (\sin 2\phi' - \sin 2\phi - \sin 2\psi' + \sin 2\psi). \quad (20)$$

For including the discrete size of the cable in the sector model, we define the final angles as

$$\begin{aligned} \phi' &= \phi + m \Delta\phi, \\ \psi' &= \psi + m \Delta\phi, \end{aligned} \quad (21)$$

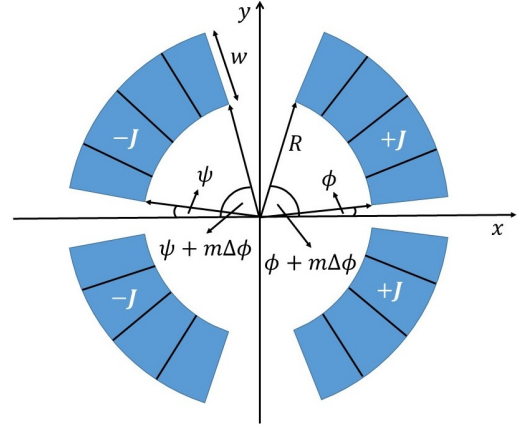


Figure 4. Asymmetric sector coil about the y -axis and symmetric about the x -axis. ϕ and ψ are the starting angles of the right and left sectors respectively. Both sectors have the bending radius R and the width w . They are composed from m turns and $\Delta\phi$ is the angle underlying the turn.

where m is the number of turns of each sector and $\Delta\phi$ is the angle underlying the turn (see Fig. 4). It is calculated as

$$\Delta\phi = \arcsin \frac{\bar{l}}{\bar{R}}, \quad (22)$$

where \bar{l} is the mean cable thickness, considered as conductor plus insulation, and $\bar{R} = R + w/2$ is the mean bending radius of the cable. Therefore, the equations (19) and (20) are rewritten as

$$B_n = \frac{\mu_0 J R_{ref}^{n-1}}{\pi n (n-2)} \left(\frac{1}{(R+w)^{n-2}} - \frac{1}{R^{n-2}} \right) \times \left[\sin n(\phi + m \Delta\phi) - \sin n\phi - (-1)^n (\sin n(\psi + m \Delta\phi) - \sin n\psi) \right] \quad (23)$$

and

$$B_2 = \frac{\mu_0 J R_{ref}}{2\pi} \ln \frac{R}{R+w} \times \left[\sin 2(\phi + m \Delta\phi) - \sin 2\phi - \sin 2(\psi + m \Delta\phi) + \sin 2\psi \right]. \quad (24)$$

The choice to work with the mean cable thickness on the mean bending radius has been done to minimize the harmonic error, due to the geometric differences between the sector coil and the real coil, which are not negligible in the FCC dipole. The maximum error on the most

sensible harmonic becomes $\Delta b_3 < 19$ units in the 16-T bending dipole and $\Delta b_3 < 11$ units in the dipole D2. In the twin-aperture layout, Eq. (23) and Eq. (24) are the harmonics generated from the right coil in the right aperture and, hereafter, we indicate them as B_n^r .

The left coil conductors are far from the right coil aperture, the region where the harmonics are computed. Therefore, we can analytically describe the left coil harmonic contribution approximating each conductor by a single current line, flowing in the center of the turn itself (see Fig. 5). This approximation brings to a maximum error of about 5%.

The contribution of the left coil, in the right aperture, is

$$\begin{aligned}
B_n^l = & -\frac{\mu_0 I R_{ref}^{n-1}}{2\pi} \sum_{i=1}^m \frac{\cos n(\pi - \theta_i)}{\rho_i^n} \\
& - \frac{\mu_0 I R_{ref}^{n-1}}{2\pi} \sum_{i=1}^m \frac{\cos n(\pi + \theta_i)}{\rho_i^n} \\
& - \frac{\mu_0 (-I) R_{ref}^{n-1}}{2\pi} \sum_{i=1}^m \frac{\cos n(\pi - \theta'_i)}{(\rho'_i)^n} \\
& - \frac{\mu_0 (-I) R_{ref}^{n-1}}{2\pi} \sum_{i=1}^m \frac{\cos n(\pi + \theta'_i)}{(\rho'_i)^n},
\end{aligned} \tag{25}$$

where ρ_i and θ_i are the polar coordinates of the current lines of the left sectors and ρ'_i and θ'_i are the polar coordinates of the current lines of the right sectors. By using Eq. (16), we get

$$\begin{aligned}
B_n^l = & -(-1)^n \frac{\mu_0 I R_{ref}^{n-1}}{\pi} \sum_{i=1}^m \frac{\cos n\theta_i}{\rho_i^n} \\
& - (-1)^n \frac{\mu_0 (-I) R_{ref}^{n-1}}{\pi} \sum_{i=1}^m \frac{\cos n\theta'_i}{(\rho'_i)^n}.
\end{aligned} \tag{26}$$

We set the versus of the currents in way that the magnetic field in the left aperture has polarity opposite than the right aperture. This is the case of the 16-T bending dipole for FCC. Instead, for the recombination dipole D2 of HL-LHC, the magnetic field must have the same polarity in the two aperture and this condition is realized if we reverse the versus of the currents in Eq. (26). The current density J , which flows in the conductors of the right coil, is linked to the current intensity I , as $J = I/S$, where S is the area of each conductor, computed as

$$S = \frac{(R+w)^2 - R^2}{2} \Delta\phi. \tag{27}$$

The polar coordinates of the current lines, $\rho_i, \theta_i, \rho'_i, \theta'_i$, are linked to the angles ϕ or ψ of the corresponding sector of the right coil, by the simple trigonometric formulas.

First, we define the polar coordinates of the current lines in the middle of each turn of the right coil as

$$\begin{aligned}
r &= R + \frac{w}{2}, \\
\gamma_i &= \phi + \left(i + \frac{1}{2}\right) \Delta\phi, \\
\gamma'_i &= \psi + \left(i + \frac{1}{2}\right) \Delta\phi,
\end{aligned} \tag{28}$$

where i is an integer number from 0 to $m-1$. Then, we set the polar coordinates of the current lines of the left coil, splitting between right and left sectors. Indeed, because the beams are counter-rotating, the left coil is mirrored to the right coil. Therefore, the left sectors of the left coil correspond to the right sectors of the right coil and the right sectors of the left coil correspond to the left sectors of the right coil.

For the left sectors of the left coil, the trigonometric formulas are

$$\begin{aligned}
\theta_i &= \arctan\left(\frac{r \sin \gamma_i}{2d + r \cos \gamma_i}\right), \\
\rho_i &= \frac{2d + r \cos \gamma_i}{\cos \theta_i},
\end{aligned} \tag{29}$$

where d is half of the inter-beam distance; while for the right sectors of the left coil we have

$$\begin{aligned}
\theta'_i &= \arctan\left(\frac{r \sin \gamma'_i}{2d - r \cos \gamma'_i}\right), \\
\rho'_i &= \frac{2d - r \cos \gamma'_i}{\cos \theta'_i}.
\end{aligned} \tag{30}$$

Equations (28), (29) and (30) require to rewrite the summation in Eq. (26), which becomes

$$\begin{aligned}
B_n^l = & -(-1)^n \frac{\mu_0 I R_{ref}^{n-1}}{\pi} \sum_{i=0}^{m-1} \frac{\cos n\theta_i}{\rho_i^n} \\
& - (-1)^n \frac{\mu_0 (-I) R_{ref}^{n-1}}{\pi} \sum_{i=0}^{m-1} \frac{\cos n\theta'_i}{(\rho'_i)^n}.
\end{aligned} \tag{31}$$

The normalized harmonics, produced in the right coil aperture by the two coils, are

$$\begin{aligned}
& b_n^{coil}(\phi_1, \psi_1, m_1, \dots, \phi_N, \psi_N, m_N) \\
& = 10^4 \frac{\sum_{p=1}^N [B_n^r(\phi_p, \psi_p, m_p) + B_n^l(\phi_p, \psi_p, m_p)]}{\sum_{p=1}^N [B_1^r(\phi_p, \psi_p, m_p) + B_1^l(\phi_p, \psi_p, m_p)]},
\end{aligned} \tag{32}$$

where N is the number of the coil sectors.

Now, we must consider the iron yoke saturation and the harmonic error due to the geometric differences between

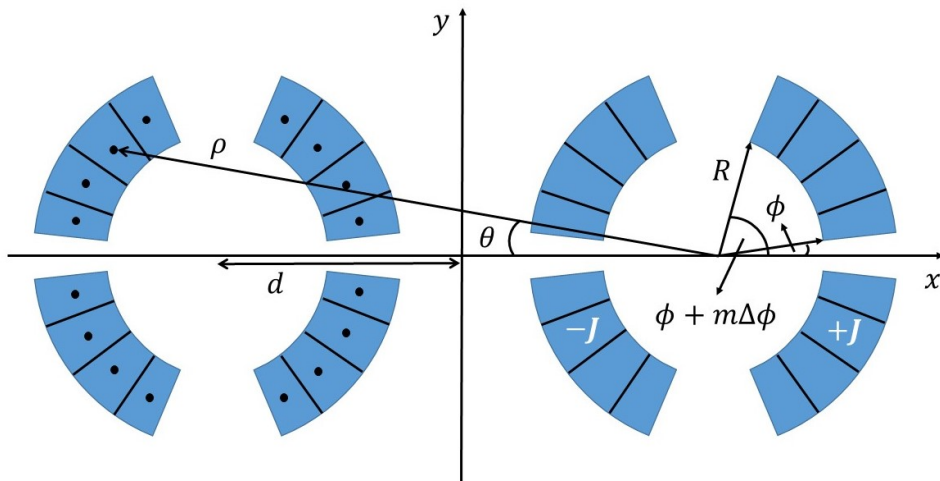


Figure 5. Twin-aperture layout. The two sector coils are mirrored, because the beams are counter-rotating. Each coil has the asymmetric cross-section about its vertical axis. The conductors of the left coil are approximated by single current lines, flowing in the center of the conductors themselves (black points); ρ and θ are the coordinates of each current line. d is half of the inter-beam distance.

the sector coil and the real coil. We observed that these contributions poorly depend from the “coordinates” of the configuration (ϕ_p, ψ_p, m_p) . Then, we can regard the shift from the model solution, $\Delta b_n^{sat+geom}$, approximately as a constant value, which can be estimated by a single FEM evaluation [3]. Therefore, the total normalized harmonics are

$$\begin{aligned} b_n(\phi_1, \psi_1, m_1, \dots, \phi_N, \psi_N, m_N) \\ = b_n^{coil}(\phi_1, \psi_1, m_1, \dots, \phi_N, \psi_N, m_N) + \Delta b_n^{sat+geom}. \end{aligned} \quad (33)$$

The quadratic sum of the total normalized harmonics is minimized by an iterative method:

1. we generate a random configuration of the left coil $(\phi_1, \psi_1, m_1, \dots, \phi_N, \psi_N, m_N)$ and compute the harmonics $B_n^l(\phi_p, \psi_p, m_p)$ in Eq. (32);
2. we numerically find a configuration of the right coil $(\phi'_1, \psi'_1, m'_1, \dots, \phi'_N, \psi'_N, m'_N)$, for whom the multipoles $B_n^r(\phi'_p, \psi'_p, m'_p)$ delete the harmonics $B_n^l(\phi_p, \psi_p, m_p)$;
3. we check the total normalized harmonics $b_n(\phi'_1, \psi'_1, m'_1, \dots, \phi'_N, \psi'_N, m'_N)$ and we stop if b_2 and b_3 are within few units (the higher order harmonics are already within one unit after the first iteration);
4. otherwise we update the contributions of the left coil $B_n^l(\phi'_p, \psi'_p, m'_p)$ and we repeat the steps 2 and 3.

IV. RESULTS

The High Luminosity upgrade of LHC requires the replacement of the superconducting magnets, before and after the interaction regions (IR) of the ATLAS and CMS experiments [37]. An important role is played by the dipoles recombining and separating the two proton beams around the IR [38]. These dipoles, D1 and D2, bend the beams in opposite directions. In particular, D2 is a twin-aperture magnet, with an aperture diameter of 105 mm and a inter-beam distance of 188 mm. The dipole must generate an integrated magnetic field of 35 Tm with the same polarity in both apertures. The coils are wound with the same Rutherford cable already used in the outer layer of the LHC bending dipole. The main features of the dipole D2 are listed in Table I. Fig. 6 shows the asymmetric coil cross-section and Fig. 7 shows the optimized shape of the iron yoke.

This dipole was designed at INFN in the last years and a short model is currently under construction by ASG Superconductors in Genoa [13]. The magnetic design was performed by the usual numerical codes, which required a computational time of the order of the seconds to evaluate both the asymmetric coil cross-section, made of 4 or 5 blocks of Rutherford cables, and the iron yoke saturation. Because the numerical algorithms took thousands of evaluations, the optimization has been time-consuming.

We reconsidered this design on the basis of the developed analytic approach and searched new coil configurations with four and five asymmetric blocks.

By using the software Wolfram Mathematica 11.3 [39], we wrote a code, where the second step of the iterative method is resolved by a differential evolution algorithm.

By performing just one iteration, we minimized the quadratic sum of the b_n^{coil} in Eq. (32) up to b_9^{coil} . In

Table I. Main features of the dipole D2.

Feature	Unit	Value
Bore magnetic field	T	4.5
Magnetic length	m	7.78
Peak field	T	5.26
Operating current	kA	12.34
Stored energy	MJ	2.28
Overall current density	A/mm ²	443
Magnet physical length	m	8.11
Aperture diameter	mm	105
Beam distance	mm	188
Operating temperature	K	1.9
Operating point on load-line	%	66.7
Multipole variation due to iron saturation	unit	< 10
Number of apertures		2
Material		NbTi
Cu/Non-Cu		1.95
No. of strands		36
Strand diameter		mm 0.825
Cable bare width		mm 15.1
Cable bare inner thickness		mm 1.362
Cable bare outer thickness		mm 1.598
Insulation azimuthal thickness		mm 0.1
Insulation radial thickness		mm 0.125

this way we generated a coil configuration to estimate, by a usual numerical code and assuming the iron yoke in Fig. 7, the shifts $\Delta b_n^{sat+geom}$ for each harmonic. We saw that only $\Delta b_2^{sat+geom}$ and $\Delta b_3^{sat+geom}$ were not negligible (about -200 units and -80 units respectively). Then, by the iterative method we minimized the quadratic sum of Eq. (33) up to b_9 for 4 sectors and b_{11} for 5 sectors, with the only non-zero terms $\Delta b_2^{sat+geom}$ and $\Delta b_3^{sat+geom}$.

Our code evaluated the asymmetric coil cross-section, made of 4 or 5 sectors, in a computational time of about 2 milliseconds, i.e. about 1000 times faster than the traditional numerical codes. The computational time of every iteration has been at maximum of about 7-8 minutes. The code stopped after about 2 iterations. This means that about every 15 minutes we had the coordinates of a possible asymmetric coil cross-section, which already considered with good approximation the iron yoke saturation (see Tab. II). Thanks to this speed we were able to scan a much higher number of possible configurations and this allowed to find more than 40 possible solutions with the coil cross-section made of 4 or 5 sectors.

We inserted in ROXIE [40] the configurations found by our code, for computing the peak fields and the operating margins, with the coil cross-section made of blocks of Rutherford cables and the iron yoke showed in Fig. 7. Fig. 8 shows the solution which best fit the specifications and Table II shows the harmonics of this configuration. The first line displays the harmonics at the nominal current, when this solution has been inserted in ROXIE. The second line shows the harmonics after a small fine tuning on the positions and on the tilts of the blocks by means of

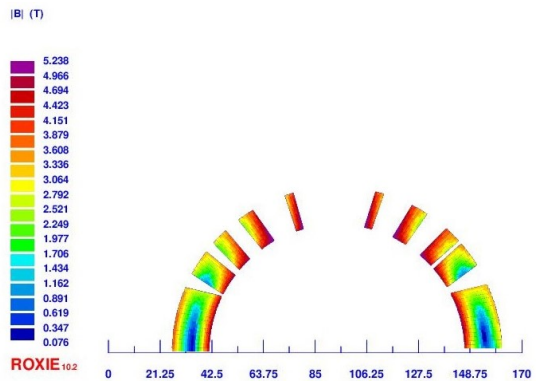


Figure 6. Asymmetric D2 coil cross-section.

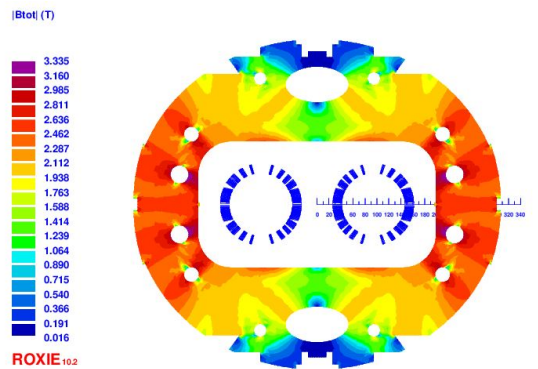


Figure 7. Iron yoke of the dipole D2.

ROXIE. The current intensity in each block is 12.72 kA, the peak field is 5.34 T and the operating point on the load-line is about 68.3%. This design has a light better field quality than the current one, but it has a light lesser margin on the load-line. These results show that in principle this configuration could be a valid alternative to the current one.

We applied the analytic method also to the design of 16-T bending dipole for the Future Circular Collider. This magnet is a twin-aperture dipole, with an aperture diameter of 50 mm and a inter-beam distance of 250 mm. The main requirements of the dipole are listed in Table III. Fig. 9 shows the asymmetric coil cross-section and Fig. 10 shows the optimized shape of the iron yoke. Each coil is made of two double pancakes, which are connected in series. Each double pancake is wound using its own conductor and this allows the third and fourth layer to have a thinner conductor. This technique is called “grading” and increases the efficiency of the outer layers to produce the main field. The main parameters of the two conductors are reported in Tab. IV. High Field (HF) conductor refers to the first and the second layer, while Low Field (LF) conductor refers to the third and the fourth layer.

The magnetic design was performed by the usual numerical codes, which required a computational time of

Table II. Normal harmonics at operating current for the dipole D2. The first line shows the harmonics of the 4-block configuration when it has been inserted in ROXIE. The second line displays the harmonics of this configuration after a small fine tuning by means of ROXIE. The last line shows the harmonics of the current 5-block configuration for a comparison.

b_2	b_3	b_4	b_5	b_6	b_7	b_8	b_9	b_{10}	b_{11}	b_{12}	b_{13}	b_{14}	b_{15}	b_{16}	b_{17}	b_{18}	b_{19}	b_{20}
8.98	3.23	9.35	2.92	0.72	-1.81	0.08	-0.66	-0.12	-0.09	-0.2	0.14	-0.29	0.41	-0.71	-1.12	0.12	-0.09	0.09
0	0	0	0	0	0	0.05	0	-0.25	0.03	-0.37	-0.02	-0.38	0.43	-0.7	-1.09	0.11	-0.10	0.09
0	0	0	0	0	0	0	0	0	-1.89	-1.80	-1.91	-1	-0.76	0.12	-0.04	0.14	0.16	-0.07

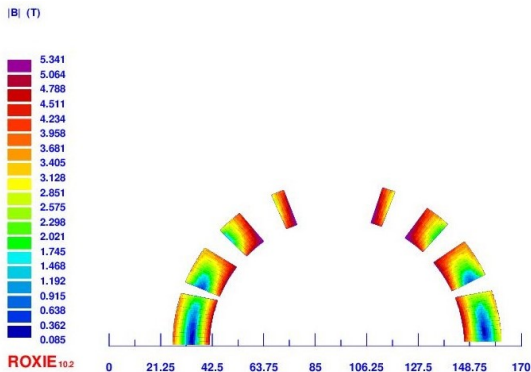


Figure 8. Alternative asymmetric D2 coil cross-section.

the order of a few seconds to evaluate both the asymmetric coil cross-section, made of 12 blocks of Rutherford cables, and the iron yoke saturation. Because the numerical algorithms took tens of thousands of evaluations, the optimization has been time-consuming one again.

Table III. Main design requirements for the FCC dipole.

Feature	Unit	Value
Material		Nb ₃ Sn
Bore magnetic field	T	16
Magnetic length	m	14.3
Aperture diameter	mm	50
Beam distance	mm	250
Iron yoke outer radius	mm	330
Operating temperature	K	1.9
Operating point on load-line	%	86
Cu/non-Cu		≥ 0.8
Maximum no. of strands		40
Field harmonics (geom/sat)	unit	≤ 3/10
Number of apertures		2

We applied our analytic approach following the same procedure of D2 and we searched new configurations with a lower or equal number of sectors. By performing just one iteration, we minimized the quadratic sum of the b_n^{coil} in Eq. (32) up to b_{10}^{coil} . In this way we generated a coil configuration to estimate, by a usual numerical code and assuming the iron yoke in Fig. 10, the shifts $\Delta b_n^{sat+geom}$ for each harmonic. We considered non-negligible only the

Table IV. Main features of the FCC conductors

Feature	Unit	HF	LF
Material		Nb ₃ Sn	Nb ₃ Sn
Cu/Non-Cu		0.82	2.08
No. of strands		22	38
Strand diameter	mm	1.1	0.7
Bare width	mm	13.2	14
Bare inner thickness	mm	1.892	1.204
Bare outer thickness	mm	2.0072	1.3261
Insulation thickness	mm	0.15	0.15
Keystone angle	°	0.5	0.5
Operating current	kA	11.44	11.44
Peak field	T	16.4	12.7
Operating point on load-line	%	86	86

terms $\Delta b_2^{sat+geom}$ and $\Delta b_3^{sat+geom}$ (about 30 units and -20 units respectively). Then, by the iterative method we minimized the quadratic sum of Eq. (33) up to b_{10} for 11-12 sectors, with the only non-zero terms $\Delta b_2^{sat+geom}$ and $\Delta b_3^{sat+geom}$. Our code evaluated the asymmetric coil cross-section up to 12 sectors in a computational time of about 6 milliseconds, i.e. once again about 1000 times faster than the traditional numerical codes. The computational time of every iteration has been at maximum of about 20 minutes. The code stopped almost always after one iteration. This means that about every 20 minutes we had the coordinates of a possible asymmetric coil cross-section, which already considered with excellent approximation the iron yoke saturation (see Tab. V). Thanks to this speed we were able to scan a much higher number of possible configurations and this allowed to find more than 30 possible solutions with the coil cross-section made of 10-12 sectors.

We inserted in ROXIE [40] the configurations found by our code, for computing the peak fields and the operating margins, with the coil cross-section made of blocks of Rutherford cables and the iron yoke showed in Fig. 10. Fig. 11 shows the solution which best fit the specifications and Table V shows the harmonics of this configuration. The first line displays the harmonics at the nominal current, when this solution has been inserted in ROXIE. The second line shows the harmonics after a small fine tuning on the positions and on the tilts of the blocks by means of ROXIE. The current intensity in each block is 11.41 kA, the peak fields are 16.4 T in the HF conductor and 12.5 T

Table V. Normal harmonics at operating current for the 16-T bending dipole. The first line shows the harmonics of the new configuration when it has been inserted in ROXIE. The second line displays the harmonics of this configuration after a small fine tuning by means of ROXIE. The last line shows the harmonics of the current configuration for a comparison.

b_2	b_3	b_4	b_5	b_6	b_7	b_8	b_9	b_{10}	b_{11}	b_{12}	b_{13}	b_{14}	b_{15}	b_{16}	b_{17}	b_{18}	b_{19}	b_{20}
0.82	-1.68	0.15	-0.66	-0.02	0.17	0.02	-0.36	0.02	1.09	0	-0.26	0	-0.05	0	-0.05	0	0	0
0	0	0	0	0	0.49	0	-0.24	0.02	1.13	0	-0.25	0	-0.05	0	-0.05	0	0	0
0.01	0.22	0.31	0.17	0.35	0.19	0.37	0.57	0.13	1.1	0.09	-0.24	0.03	-0.02	0	-0.06	0	0	0

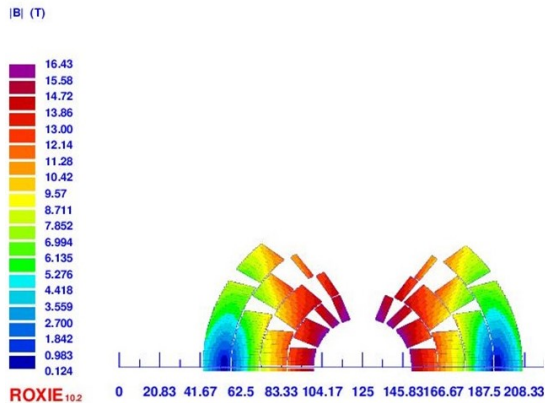


Figure 9. Asymmetric coil cross-section for the FCC bending dipole.

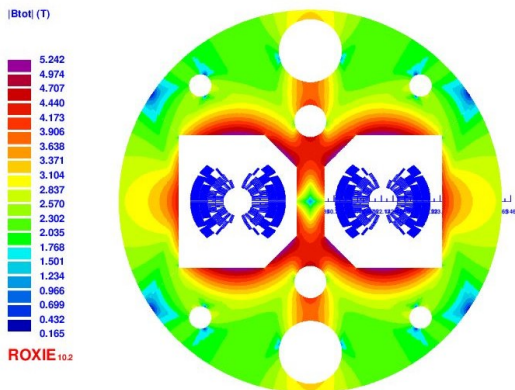


Figure 10. Iron yoke of the FCC bending dipole.

in the LF conductor, the operating points on the load-line are about 86% for the HF conductor and about 85% for the LF conductor. This design has a light better field

quality than the current one and it has a light higher margin on the load-line in the LF conductor. These results show that in principle this configuration could be a valid alternative to the current one.

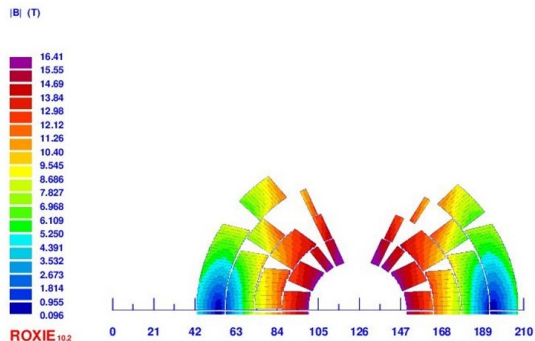


Figure 11. Alternative asymmetric coil cross-section for the FCC bending dipole.

V. CONCLUSIONS

We developed an extension of the sector model for the magnetic optimization of the twin-aperture $\cos\theta$ superconducting dipoles. It enables to minimize the magnetic cross-talk by finding the asymmetric coil configurations and by considering the iron yoke saturation. This analytic method allows a very fast computation of the field harmonics with respect to the conventional optimization tools (about 10^3 times faster). The improved speed allows to perform a much larger scan over the possible coil cross-sections and so to increase the possibilities to find the coil layout which best fits the requirements. This method was applied to two different magnets and for both it allowed to find new configurations, which could be a valid alternative to the current ones.

[1] K. H. Mess et al., *Superconducting Accelerator Magnets*, World Scientific (1996).
 [2] H. Brechna, *Superconducting Accelerator Systems*, Springer (1973).
 [3] S. Russenschuck, *Field Computation for Accelerator Magnets: Analytical and Numerical Methods for Elec-*

tromagnetic Design and Optimization (Wiley, Weinheim, 2010).
 [4] A. McInturff et al., Proc. Part. Accel. Conf., 1997, pp. 3212-3214.
 [5] R. Benjerdset et al., Proc. Part. Accel. Conf., 2001, pp. 208-210.

- [6] P. Ferracin et al., *IEEE Trans. Appl. Supercond.*, Vol. 20, no. 3, pp. 292-295 (2010).
- [7] A. Milanese et al., *IEEE Trans. Appl. Supercond.*, Vol. 22, no. 3, 4002604 (2012).
- [8] G. Montenegro et al., *IEEE Trans. Appl. Supercond.*, Vol. 29, no. 5, 4002906 (2019).
- [9] D. Schoerling and A. Zlobin, *Nb₃Sn Accelerator Magnets: Designs, Technologies and Performance*, Springer (2019).
- [10] O. S. Bruning et al., *LHC design report*, CERN-2004-003 (CERN, Geneva, 2004).
- [11] S. Farinon et al., *IEEE Trans. Appl. Supercond.*, Vol. 26, no. 4, 4001504 (2016).
- [12] P. Fabbri et al., *IEEE Trans. Appl. Supercond.*, Vol. 8, no. 3, 4000105 (2018).
- [13] A. Bersani et al., *IEEE Trans. Appl. Supercond.*, Vol. 29, no. 5, 4003305 (2019).
- [14] G. Apollinari et al., *High-Luminosity Large Hadron Collider (HL-LHC). Technical Design Report V. 0.1*, CERN-2017-007 (CERN, Geneva, 2017).
- [15] A. Abada et al. (FCC Study), *Eur. Phys. J. C*, Vol. 79, no. 6, 474 (2019).
- [16] A. Abada et al. (FCC Study), *Eur. Phys. J. ST*, Vol. 228, no. 2, pp. 261-623 (2019).
- [17] A. Abada et al. (FCC Study), *Eur. Phys. J. ST*, Vol. 228, no. 4, pp. 755-1107 (2019).
- [18] A. Abada et al. (FCC Study), *Eur. Phys. J. ST*, Vol. 228, no. 5, pp. 1109-1382 (2019).
- [19] D. Tomasini et al., *IEEE Trans. Appl. Supercond.*, Vol. 27, no. 4, 4000405 (2017).
- [20] D. Tomasini et al., *IEEE Trans. Appl. Supercond.*, Vol. 28, no. 3, 4001305 (2018).
- [21] D. Schoerling et al., *IEEE Trans. Appl. Supercond.*, Vol. 29, no. 5, 4003109 (2019).
- [22] C. Lorin et al., *IEEE Trans. Appl. Supercond.*, Vol. 27, no. 4, 4001405 (2017).
- [23] C. Lorin et al., *IEEE Trans. Appl. Supercond.*, Vol. 28, no. 3, 4005005 (2018).
- [24] M. Segreti et al., *IEEE Trans. Appl. Supercond.*, Vol. 29, no. 5, 4000404 (2019).
- [25] F. Toral et al., *IEEE Trans. Appl. Supercond.*, Vol. 27, no. 4, 4001105 (2017).
- [26] F. Toral et al., *IEEE Trans. Appl. Supercond.*, Vol. 28, no. 3, 4004305 (2018).
- [27] B. Auchmann et al., *IEEE Trans. Appl. Supercond.*, Vol. 28, no. 3, 4000705 (2018).
- [28] G. Montenero et al., *IEEE Trans. Appl. Supercond.*, Vol. 28, no. 3, 4002805 (2018).
- [29] M. Sorbi et al., *IEEE Trans. Appl. Supercond.*, Vol. 27, no. 4, 4001205 (2017).
- [30] V. Marinozzi et al., *IEEE Trans. Appl. Supercond.*, Vol. 28, no. 3, 4004205 (2018).
- [31] B. Caiiffi et al., *IEEE Trans. Appl. Supercond.*, Vol. 28, no. 4, 4006704 (2018).
- [32] R. Valente et al., *IEEE Trans. Appl. Supercond.*, Vol. 29, no. 5, 4003005 (2019).
- [33] A. Devred, *1999 Review of Superconducting Dipole and Quadrupole Magnets for Particle Accelerators* (CEA DAPNIA/STCM 99-24, France, 1999).
- [34] Bailey R., *Proceedings of the CAS-CERN Accelerator School: Superconductivity for Accelerators*, CERN-2014-005 (CERN, Geneva, 2014).
- [35] F. Borgnolutti et al., *IEEE Trans. Appl. Supercond.*, Vol. 20, no. 3, pp. 1790-1793 (2010).
- [36] A. Louzguiti et al., *IEEE Trans. Appl. Supercond.*, Vol. 29, no. 5, 4000805 (2019).
- [37] L. Bottura et al., *IEEE Trans. Appl. Supercond.*, Vol. 22, no. 3, 4002008, (2012).
- [38] E. Todesco et al., *IEEE Trans. Appl. Supercond.*, Vol. 24, no. 3, 4003305 (2014).
- [39] Wolfram Research, Inc., *Mathematica*, Version 11.3, Champaign, IL (2017).
- [40] S. Russenschuck, *ROXIE - A computer code for the integrated design of accelerator magnets*, CERN-LHC Proj. Rep. 276 (CERN, Geneva, 1999).